Effects of laser frequency chirp on modal noise in short-range radio over multimode fiber links

Visani, Davide; Tartarini, Giovanni; Petersen, Martin Nordal; Faccin, Pier; Tarlazzi, Luigi

Published in:
Applied Optics

Link to article, DOI:
10.1364/AO.49.001032

Publication date:
2010

Document Version
Publisher's PDF, also known as Version of record

Effects of laser frequency chirp on modal noise in short-range radio over multimode fiber links

Davide Visani,[1] Giovanni Tartarini,[1,*] Martin N. Petersen,[2] Pier Faccin,[3] and Luigi Tarlazzi[3]

[1]Dipartimento di Elettronica, Informatica e Sistemistica, Università di Bologna, Viale Risorgimento 2, 40136 Bologna, Italy

[2]DTU Fotonik, Institut for Fotonik Networks Technology and Service Platforms, Danmarks Tekniske Universitet, Arsteds Plads, Lyngby, Denmark

[3]Andrew Wireless Systems S.r.l., Via De Crescenzi 40, 48018 Faenza, Italy

*Corresponding author: giovanni.tartarini@unibo.it

Received 30 September 2009; revised 30 December 2009; accepted 24 January 2010; posted 25 January 2010 (Doc. ID 117946); published 19 February 2010

An important effect of the frequency chirp of the optical transmitter in radio over multimode fiber links is put into evidence experimentally and modeled theoretically for the first time, to our knowledge. This effect can have an important impact in short-range connections, where, although intermodal dispersion does not generally cause unacceptable limitations to the transmittable bandwidth, the presence of modal noise must be accurately kept under control, since it determines undesired real-time fluctuations of the link. © 2010 Optical Society of America

OCIS codes: 060.0060, 060.5625, 060.2360, 060.4510.

1. Introduction

One of the challenges of many optical systems and subsystems manufacturers has been to offer competitive solutions, in terms of cost and performance effectiveness, to satisfy the new attention that over the past years has been devoted to multimode fibers (MMF) as a candidates for last mile applications.

Applying the large core MMF instead of traditional standard single-mode fiber (SMF) brings advantages, such as simplified fiber-to-fiber connecting and splicing, enabling the use of cost-effective surface-emitting lasers (VCSELs) [1]. At the same time, since MMFs have been extensively deployed in the past years in local area, metropolitan area, and/or in-building networks, this transmission medium is, in many cases already present and needs only to be appropriately exploited. In this context, recent works report on the use of MMF for both cost-effective analog radio-over-fiber (RoF) applications [2], as well as for digital communication links providing speeds of several gigabytes per second [3].

It must be taken into account, however, that employing MMF as a transmission medium comes with the price of an increased rate of signal deterioration. For example, since the signal in an MMF is carried by several modes, the differences in modal group velocities give rise to intermodal dispersion and, thus, intersymbol interference in digital systems or distortions in RoF systems. The impact of detrimental effect increases when the MMF transmitted distance assumes values of a few kilometers. Attempts have been made to reduce these effects using either offset, central, or angled launch techniques [4,5]; all these methods work on the principle of exciting mainly modes with similar propagation characteristics and, consequently, reducing the intermodal dispersion in the MMF.

In many practical cases, however, the distances that must be covered by MMF spans do not exceed a few hundred meters. In these cases, intermodal dispersion does not generally constitute a major limiting effect, since a transmission bandwidth of some

0003-6935/10/061032-09$15.00/0

gigahertz is typically available with the simple exploitation of the baseband of the MMF transfer function. With the aim to fully exploit the potentialities of such a scenario, the effects of modal noise have to be taken into account. Modal noise appears as random fluctuations of the received light intensity, and can have an important impact on the characteristics of the received signal also in the cases when short MMF lengths are considered. Modal noise comes as a consequence of time variations of the speckle pattern at the output plane of the MMF [6–10]. One of the causes of modal noise is given by the variation in time of quantities such as environmental temperature or mechanical fiber stress, which determines the fluctuation of the optical phase differences among the modes guided by the MMF.

One possible solution, which leads to a strong reduction of modal noise, is the use of optical transmitters based on light-emitting diodes (LEDs). In this case, the optical source exhibits a low degree of coherence, and the optical phase relationships among the different modes are lost after a relatively short distance propagated in the MMF. However, with the aim of realizing cost-effective solutions, it is mandatory to use direct intensity modulation (IM) of the optical source, i.e., without the use of external expensive optical modulators, as well as direct detection (DD) of the modulated light performed by a photodiode (PD). LEDs in this context exhibit unacceptable limitations, since their modulation bandwidth is limited to some hundreds of megahertz [11].

The use of optical transmitters (TX) based on direct modulated laser diodes (LD) is then attractive because it allows overcoming this limitation. An additional beneficial aspect of choosing such a solution is that this kind of optical TXs are already available, being widely used in the current deployment of RoF systems that are based on SMF. However, the very high coherence of a LD emission brings back modal noise as a possible cause of system impairments and, consequently, the necessity to keep the undesired time fluctuations determined by modal noise on the system's transmission characteristics under control.

In this work, we devote our attention to radio-over-multimode-fiber (RoMMF) links based on the direct modulation of a LD, and we show that LDs' frequency chirping plays a very important role in determining the impact of modal noise on the characteristics of the received signal. This result must be taken into consideration at the design stage of this kind of optical system because, unlike the case of typical radio-over-single-mode-fiber links, where the combined effect of LDs' frequency chirp and chromatic dispersion of SMFs becomes a primary cause of reduction in performance after some tens of kilometers [12]; in this case, the detrimental effect of the LDs' frequency chirp cannot be neglected, even for short-range (a few hundred meters long) RoMMF links.

An analysis of RoMMF links has already been performed in [13], which included the possible influence of frequency chirp in the RoF TX on modal noise. Modal noise was studied with reference to a single speckle of the pattern at the output of the MMF, performing an analysis of the ratio between the standard deviation and the average value of the light intensity of such a single speckle (the so-called speckle contrast). The approach proposed here is different from the one just cited, since the evaluation of the modal noise impact in this case refers to the overall light intensity collected by the PD at the receiving end. Consequently, it permits an immediate comparison of the results from the numerical model with the experimentally measured results. The experimental behavior can, in fact, be characterized by observing the undesired fluctuations of the amplitude of the radio frequency (RF) modulating signal detected at the receiver side in physical RoMMF links. Moreover, since our analysis is focused on short-range links, we can make certain assumptions regarding the optical phases and group delays of the propagating modes, which, as is illustrated in Section 3, allow us to simulate some observed behaviors of the demodulated RF signal that cannot be put into evidence with the approach developed in [13].

The work is organized as follows. In Section 2, the RoMMF system considered will be theoretically described through the development of a rigorous mathematical model, and the influence of the frequency chirp of the LD on the modal noise will be put into evidence. In Section 3, a comparison between the modeled and experimental results obtained with reference to real RoMMF links will be shown and commented upon. Finally, conclusions will be drawn in Section 4.

2. Theoretical Model and Numerical Results

As stated before, we are considering a direct intensity modulated LD and we must, therefore, take into account the phenomenon of LD frequency chirping. If we consider only the adiabatic chirp, which, in general, prevails over the so-called transient chirp [14], we obtain, in the case of a sinusoidal LD modulation, an electrical field that assumes the following form:

$$E(t) = E_0\sqrt{1 + m_I\cos(2\pi f_c t)} \cdot \exp\left[j\left(2\pi f_0 t + \frac{K_f I_{\mathrm{RF}}}{f_c}\sin(2\pi f_c t)\right)\right], \quad (1)$$

where E_0 is the field's amplitude without RF modulation, K_f is its frequency modulation index or adiabatic chirp factor (usually expressed in MHz/mA), f_0 is the optical carrier's frequency, m_I is the optical modulation index (OMI), f_c is the frequency carrier of the RF modulating signal, and I_{RF} is its amplitude.

The electrical field, which is typically guided out of the LD by an SMF pigtail, is then coupled to the MMF and, consequently, is divided into its propagating modes. The field at the input section is then expressed by

$$E_{\text{in}}(t,z=0)=\sum_{m=1}^{N_M}A_m e_m(x,y)\sqrt{1+m_I\cos(2\pi f_c t)}\cdot\exp\left[j\left(2\pi f_0 t+\frac{K_f I_{\text{RF}}}{f_c}\sin(2\pi f_c t)\right)\right], \tag{2}$$

where N_M is the number of propagating modes of the MMF, $e_m(x,y)$ is the normalized field of the mth propagating mode, and A_m its weight coefficient, which depends on the launch condition. x and y are the transversal spatial coordinates, while z is the longitudinal coordinate.

In this way it is possible to determine the output electrical field after propagation in a MMF span of length L:

$$E_{\text{out}}(t,z=L)=\sum_{m=1}^{N_M}A_m e_m(x,y)\cdot\sqrt{1+m_I\cos(2\pi f_c(t-\tau_m L))}\cdot\exp\left[j\left(2\pi f_0 t-\beta_m L+\phi_m(t,L)+\frac{K_f I_{\text{RF}}}{f_c}\sin(2\pi f_c(t-\tau_m L))\right)\right], \tag{3}$$

where β_m is the propagation constant of the mth mode, while τ_m is its group delay per meter. The time-varying function $\phi_m(t,L)$ takes into account the slow phase variation of the mth mode with respect to the nominal phase shift $\beta_m z$.

An important assumption has been made in our numerical model with reference to the time behavior of $\phi_m(t,L)$. Considering the case of the featured RoMMF links, we can, in fact, assume that the undesired fluctuations of the received optical power must be caused by the "typical" slow variations, driven by environmental temperature and/or fiber stress that are experienced by the MMF fiber span during day operations. Indeed, the output field characteristics of the optical emission of the LDs used in the experiments, like the emission wavelength, output power level, and polarization state, have been found very stable over time. This is a consequence of the quality of the distributed feedback (DFB) LD devices that the RoF TX used in the experiments are based on.

The time variations of the external quantities mentioned above influence the transmission characteristics of the optical fiber, because they determine corresponding time variations of the refractive index of the fiber itself, which, in turn, determines the time variations of the phase in the different modes, $\phi_m(t,L)$. By assuming that the phase of each mode is influenced by the same time fluctuations of the refractive index, the time evolution of the various $\phi_m(t,L)$ contributions can be modeled. However, because, in general, the phase of each mode will be affected in a different way by the external variation, each $\phi_m(t,L)$ contribution was multiplied by a random scale factor and a random initial start value was assumed.

Using the DD technique, we have a received current $i_{\text{out}}(t,L)$ proportional to the optical power received on the photodiode surface S_{PD} (we assume a PD's responsivity equal to 1):

$$\begin{aligned}i_{\text{out}}(t,L)=\int_{S_{\text{PD}}}|E_{\text{out}}(t,z=L)|^2\mathrm{d}S=\sum_{m=1}^{N_M}\sum_{n=1}^{N_M}A_m A_n\\ \cdot\int_{S_{\text{PD}}}e_m(x,y)\cdot e_m^*(x,y)\mathrm{d}S\\ \cdot\sqrt{1+m_I\cos(2\pi f_c(t-\tau_m L))}\\ \cdot\sqrt{1+m_I\cos(2\pi f_c(t-\tau_n L))}\\ \cdot\exp[j(\beta_n-\beta_m)L]\\ \cdot\exp\left[-j\left((\phi_n(t,L)-\phi_m(t,L))\right.\right.\\ +\frac{K_f I_{\text{RF}}}{f_c}(\sin(2\pi f_c(t-\tau_n L))\\ \left.\left.-\sin(2\pi f_c(t-\tau_m L))\right)\right].\end{aligned} \tag{4}$$

We emphasize that, in determining the expression of $i_{\text{out}}(t,L)$, we have neglected the influence of the phase noise of the laser source. This would not have been correct if sources exhibiting a low level of coherence (such as a Fabry–Perot laser or a LED) were used. In our case, however, we utilized DFB LDs, which, regardless of the value of the adiabatic chirp factor K_f, always exhibited a linewidth of less than 10 MHz, resulting in a coherence time τ_c larger than 100 ns. This value is much higher than the maximum theoretical difference between group delays in our MMFs, which, for a fiber with a length $L=300$ m, like the one utilized in our experiments, is $|\tau_m-\tau_n|_{MAX}\cdot L\approx 1\,\text{ns}\ll\tau_c$. The DFB LDs can, therefore, be assumed as sinusoidal sources not affected by phase noise. This hypothesis of high coherence leads to the maximum possible interference between modes.

Approximating in Eq. (4) the product of square roots to the first order and separating the summation among the modes with equal subscripts and the one performed among the modes with different subscripts, we obtain, after some algebra:

$$\begin{aligned}i_{\text{out}}(t,L)=\sum_{n=1}^{N_M}A_m^2 b_{mm}(1+m_I\cos(2\pi f_c(t-\tau_m L)))\\ +\sum_{m=1}^{N_M}\sum_{n=m+1}^{N_M}2A_m A_n b_{mn}\\ \cdot[1+m_I\cos(\pi f_c\Delta\tau_{g,mn})\cos(\pi f_c(\tau_m+\tau_n)L)]\\ \cdot[\cos(x_{mn}\cos(2\pi f_c t-\pi f_c(\tau_m+\tau_n)L))\\ \cdot\cos(\Delta\varphi_{mn}(t))\\ +\sin(x_{mn}\cos(2\pi f_c t-\pi f_c(\tau_m+\tau_n)L))\\ \cdot\sin(\Delta\varphi_{mn}(t))],\end{aligned} \tag{5}$$

with

$$b_{mn} = \int_{S_{PD}} e_m(x,y) \cdot e_n^*(x,y) \mathrm{d}S, \tag{6}$$

$$\Delta\tau_{g,mn} = (\tau_m - \tau_n)L, \tag{7}$$

$$\Delta\varphi_{mn}(t) = (\beta_m - \beta_n)L + (\phi_m(t,L) - \phi_n(t,L)), \tag{8}$$

$$x_{mn} = 2\pi K_f I_{RF} \Delta\tau_{g,mn} \frac{\sin(\pi f_c \Delta\tau_{g,mn})}{\pi f_c \Delta\tau_{g,mn}}. \tag{9}$$

The term b_{mn} in Eq. (6) is the scalar product between the normalized fields of two modes and, in theory, it should be equal to 1 for equal subscripts ($m = n$), while it should be zero for different subscripts ($m \neq n$). Unfortunately, while we can consider b_{mm} to be approximately equal to 1, due to factors such as imperfect coupling between fiber and photodiode and the finite area of the photodiode, this scalar product is, in most cases, not zero also when $m \neq n$, and it is therefore important to take it into account.

In the Section 3, details will be given on how estimated values for the different b_{mn}'s have been determined, in order for them to be used as input parameters into our simulation program.

Now, to determine the received photocurrent at the carrier frequency f_c and the DC, we need to extract the corresponding components from Eq. (5). Using the Fourier expansion for the expressions $\cos(x_{mn} \cdot \cos(2\pi f_c t - \pi f_c(\tau_m + \tau_n)z))$ and $\sin(x_{mn} \cdot \cos(2\pi f_c t - \pi f_c \cdot (\tau_m + \tau_n)z))$ through Bessel functions, and neglecting Bessel functions of order higher that 1, we get, for the DC component of the received photocurrent,

$$I_{DCout}(t) = I_{DCout} + \Delta I_{DCout}(t), \tag{10}$$

with

$$I_{DCout} = \sum_{m=1}^{N_M} A_m^2, \tag{11}$$

$$\Delta I_{DCout}(t) = \sum_{m=1}^{N_M} \sum_{n=m+1}^{N_M} 2A_m A_n b_{mn} J_0(x_{mn}) \cdot \cos(\Delta\varphi_{mn}(t)), \tag{12}$$

while we get, for the *RF* component of the received photocurrent,

$$i_{RFout}(t) = (A_c + B_c)\cos(2\pi f_c t) + (A_s + B_s)\sin(2\pi f_c t), \tag{13}$$

with

$$A_c = m_I \sum_{m=1}^{N_M} A_m^2 \cos(2\pi f_c \tau_m L), \tag{14}$$

$$A_s = m_I \sum_{m=1}^{N_M} A_m^2 \sin(2\pi f_c \tau_m L), \tag{15}$$

$$B_c = \sum_{m=1}^{N_M} \sum_{n=m+1}^{N_M} 2A_m A_n b_{mn} C_{mn}(t) \cos(\pi f_c(\tau_m + \tau_n)L), \tag{16}$$

$$B_s = \sum_{m=1}^{N_M} \sum_{n=m+1}^{N_M} 2A_m A_n b_{mn} C_{mn}(t) \sin(\pi f_c(\tau_m + \tau_n)L), \tag{17}$$

and where

$$C_{mn}(t) = m_I \cos(\pi f_c \Delta\tau_{g,mn}) \cdot J_0(x_{mn}) \cdot \cos(\Delta\varphi_{mn}(t)) + 2J_1(x_{mn}) \cdot \sin(\Delta\varphi_{mn}(t)). \tag{18}$$

As will be illustrated at the end of the present section, the term $C_{mn}(t)$ defined in Eq. (14) has a crucial role in illustrating the phenomenon that we intend to point out on this paper.

If we now consider short fiber lengths (up to a few hundred meters) and radio carrier frequencies that are well contained within the 3 dB bandwidth of the MMF fiber (typically up to a few gigahertz), it is possible to consider the group delays of the different modes as being very close to each other. In this way, we can make an approximation considering that each τ_m in the previous equations is approximately equal to an appropriate mean value. The approximation will not be applied to the quantity $\Delta\tau_{g,mn}$ contained in x_{mn} [see Eq. (9)] because, in this case, an infinite relative error would be introduced. Then Eq. (13) becomes

$$i_{RFout}(t) = (I_{RFout} + \Delta I_{RFout}(t))\cos(2\pi f_c(t - \tau_g L)), \tag{19}$$

with

$$I_{RFout} = m_I \sum_{m=1}^{N_M} A_m^2 = m_I \cdot I_{DCout}, \tag{20}$$

$$\Delta I_{RFout}(t) = \sum_{m=1}^{N_M} \sum_{n=m+1}^{N_M} 2A_m A_n b_{mn} [m_I \cdot J_0(x_{mn}) \cdot \cos(\Delta\varphi_{mn}(t)) + 2J_1(x_{mn}) \cdot \sin(\Delta\varphi_{mn}(t))], \tag{21}$$

where τ_g is the aforesaid equivalent mean value of the group delays of the modes.

To put into evidence the dependence of $\Delta I_{RFout}(t)$ from the transmitter chirp factor K_f, we will now proceed with an approximation, which would be applicable only for a very low value of x_{mn}, but which is useful because it allows us to perform a qualitative reasoning. We can, in fact, approximate the Bessel

functions contained in Eqs. (12) and (21) at the first order ($J_0(x) \cong 0$, $J_1(x) \cong x/2$) obtaining

$$\Delta I_{\mathrm{DCout}}(t) \approx \sum_{m=1}^{N_M} \sum_{n=m+1}^{N_M} 2A_m A_n b_{mn} \cdot \cos(\Delta\varphi_{mn}(t)), \tag{22}$$

$$\begin{aligned}\Delta I_{\mathrm{RFout}}(t) &\approx \sum_{m=1}^{N_M} \sum_{n=m+1}^{N_M} 2A_m A_n b_{mn} [m_I \cdot \cos(\Delta\varphi_{mn}(t)) \\ &\quad + 2\pi K_f I_{\mathrm{RF}}(\tau_m - \tau_n) L \cdot \sin(\Delta\varphi_{mn}(t))] \\ &= m_I \Delta I_{\mathrm{DCout}}(t) + 2\pi K_f \cdot I_{\mathrm{RF}} \cdot L \\ &\quad \cdot \sum_{m=1}^{N_M} \sum_{n=m+1}^{N_M} 2A_m A_n b_{mn}(\tau_m - \tau_n) \\ &\quad \cdot \sin(\Delta\varphi_{mn}(t)). \end{aligned} \tag{23}$$

With this approximation we point out that the DC component is not dependent on the chirp factor of the laser, while the RF component is composed of two terms: the first one is proportional to $\Delta I_{\mathrm{DCout}}(t)$ with proportionality factor m_I, while the second one is a sum of quantities similar to Eq. (22) but with the $\cos(*)$ substituted by a $\sin(*)$. This second term is multiplied by a constant factor equal to $2\pi \cdot K_f \cdot I_{\mathrm{RF}} L$ and, considering the typical values of the quantities involved, normally prevails over the first one. Furthermore, it is proportional to m_I since the input current I_{RF} can be written as $I_{\mathrm{RF}} = m_I \cdot I_0$, with the I_0 constant DC term proportional to the difference between the bias current and the threshold current of the LD considered.

The presence of this term can be seen as a phase-modulation-to-intensity-modulation (PM-IM) conversion due to modes' interference, which increases with the frequency modulation chirp factor K_f of the laser source [in the simplified case of Eq. (23), it is proportional to K_f]. This phenomenon becomes negligible if K_f is so small that the first addend of Eq. (23) overcomes the second one. This is possible when we use an external modulator and, in this case, we can understand from Eq. (23) that $\Delta I_{\mathrm{RFout}}(t)$ and $\Delta I_{\mathrm{DCout}}(t)$ are practically in phase. This result will be underlined also in Section 3.

We will now show a result coming from the application of this numerical model, which will be confirmed in Section 3 experimental measurements.

Figure 1 shows a typical computed time fluctuation of the RF component of the received photocurrent normalized to the OMI, $\Delta I_{\mathrm{RFout}}(t)/m_I$, and of the DC component $\Delta I_{\mathrm{DCout}}(t)$. We chose to represent the quantity $\Delta I_{\mathrm{RFout}}(t)/m_I$ instead of $\Delta I_{\mathrm{RFout}}(t)$, since, from the inspection performed above of Eq. (23), which approximates Eq. (21), we can conclude that this last quantity is very weakly dependent on m_I, while it strongly depends on the chirp factor of the laser and on the properties of the fiber. This result is also confirmed by experimental results, so we will utilize $\Delta I_{\mathrm{RFout}}(t)/m_I$ also in the figures in Section 3.

The simulation result shown in Fig. 1 refers to the experimental configuration of the "high-frequency chirping" transmitter case of the real RoMMF link that will be described in detail in Section 3. In this figure, the behavior of the optical phase $\varphi_m(t, L)$ referred to a generic one of the propagating modes of the fiber is also reported in order to put into evidence its correlation with the fluctuations of RF and DC. It can be noted that, starting from the instant $t = 0$s and arriving to $t \approx 400$ s, $\varphi_m(t, z)$ exhibits an upward sloping behavior. This allows us to observe the effect of the frequency chirp of the laser source. In fact, looking at the expression of $C_{mn}(t)$ given by Eq. (14), we have that the nonzero value of the coefficient K_f, which is contained in x_{mn} [see Eq. (9)] determines a nonzero value for the term that, in $C_{mn}(t)$, is proportional to $\sin(\Delta\varphi_{mn}(t))$ and this results in the fact that $\Delta I_{\mathrm{DCout}}(t)$ [given by Eq. (12)] and $\Delta I_{\mathrm{RFout}}(t)$ [given by Eq. (17)] are not in phase. On the contrary, due to the presence of the term proportional to K_f, $\Delta I_{\mathrm{DCout}}(t)$ exhibits maxima in correspondence to the upward slopes of $\Delta I_{\mathrm{RFout}}(t)$. It can be also seen that, for $t \approx 400$ s, in a span of time of about 200 s, corresponding to a stationary behavior of $\varphi_m(t, L)$, $\Delta I_{\mathrm{RFout}}(t)$ and $\Delta I_{\mathrm{DCout}}(t)$ tend to be relatively stationary (i.e., they both tend to exhibit reduced fluctuations). Subsequently, starting from the instant $t \approx 600$ s and arriving to $t \approx 1000$ s, $\varphi_m(t, L)$ exhibits a downward sloping behavior and, as a result, $\Delta I_{\mathrm{RFout}}(t)$ and $\Delta I_{\mathrm{DCout}}(t)$ are again not in phase, and $\Delta I_{\mathrm{DCout}}(t)$ now exhibits maxima in correspondence to the downward slopes of $\Delta I_{\mathrm{RFout}}(t)$.

Note in particular that the fluctuations described by the function $\Delta I_{\mathrm{RFout}}(t)$ result in undesired fluctuations of the magnitude G_{RF} of the link gain, which is one fundamental quantity that has to be considered for design purposes in analog modulated RoF links. Utilizing the previously defined quantities, we can in

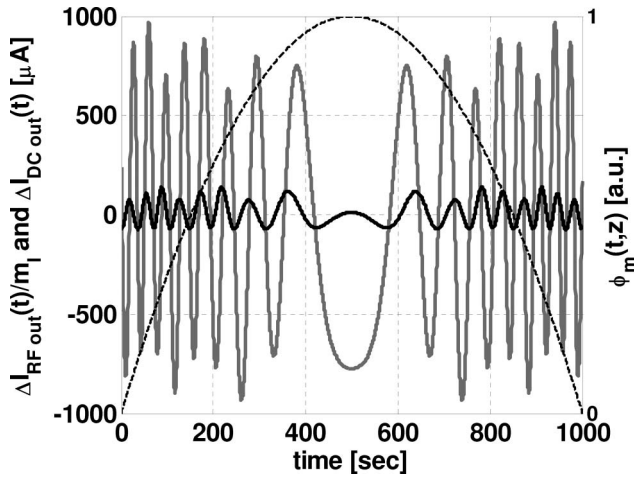

Fig. 1. Simulated behavior of the time fluctuations due to modal noise on the amplitude of the received photocurrent (DC term, black curve; RF term, $f_{\mathrm{RF}} = 1$ GHz, gray curve) for the RoMMF system considered and of the optical phase $\varphi_m(t, z = L)$ of a generic propagating mode (dashed curve). The RoF TX used is assumed to operate in the C band and to exhibit $K_f = 220$ MHz/mA.

fact write

$$G_{\mathrm{RF}} = \left| \frac{I_{\mathrm{RFout}} + \Delta I_{\mathrm{RFout}}(t)}{I_{\mathrm{RF}}} \right|^2, \tag{24}$$

and, consequently, represent in logarithmic units the maximum extension of the undesired fluctuations of G_{RF} as

$$\begin{aligned} \Delta G_{\mathrm{RF}MAX} &= 10 \cdot \log_{10} \left| \frac{[I_{\mathrm{RFout}} + \Delta I_{\mathrm{RFout}}(t)]_{MAX}}{[I_{\mathrm{RFout}} + \Delta I_{\mathrm{RFout}}(t)]_{MIN}} \right|^2 \\ &= 20 \cdot \log_{10} \left(\frac{I_{\mathrm{RFout}}/m_I + [\Delta I_{\mathrm{RFout}}(t)/m_I]_{MAX}}{I_{\mathrm{RFout}}/m_I + [\Delta I_{\mathrm{RFout}}(t)/m_I]_{MIN}} \right), \end{aligned} \tag{25}$$

since the fluctuations are always lower than the mean value.

So, if in the example of Fig. 1, the mean received DC $\Delta I_{\mathrm{DCout}} = 6\,\mathrm{mA}$ (corresponding to 7.8 dBm of received optical power), since $\Delta I_{\mathrm{RFout}}(t)/m_I$ varies approximately between −1000 and 1000 μA, we obtain $\Delta G_{\mathrm{RF}MAX} = 20 \cdot \log_{10}(7000/5000) \cong 3\,\mathrm{dB}$.

In Section 3, the particular behavior described with reference to Fig. 1 will be confirmed by experimental results, and a practical consequence on the relationship between the value of K_f and the impact of modal noise in RoMMF systems will be illustrated.

3. Experimental Results and Comparison

The optical (IM–DD) system that we utilized for our measurements is depicted in Fig. 2. An RF sinusoidal tone, generated by a vector network analyzer (VNA), modulates an optical carrier, giving rise to a RoF signal. This RoF signal is coupled to 300 m of SYSTIMAX LazrSPEED 550 graded index 50/125 MMF and reaches a RoF receiver (RX) based on a InGaAs positive-intrinsic-negative (PIN) PD. The output port of the RoF RX is connected to the VNA itself, while the DC component of the received current is measured through a multimeter.

As schematized in Fig. 2, we performed different measurements by putting the RoMMF link in the same operating conditions, but choosing three different ways to generate the RoF signal. In fact, we utilized two RoF TXs (TX_1 and TX_2 in Fig. 2), both based on a DFB LD in a direct modulation scheme, which exhibited different adiabatic chirp factors ($K_f = K_{f1} = 220\,\mathrm{MHz/mA}$ and $K_f = K_{f2} = 30\,\mathrm{MHz/mA}$, respectively). In addition to these, as a third configuration, we used a RoF TX operating in continuous-wave (CW) mode followed by an electro-optical Mach–Zehnder modulator (MZM) to perform the external RF modulation of the optical carrier. The MZM utilized was a dual output analog optical modulator, and its frequency chirp $K_f = K_{f,MZM}$ can be estimated to be lower than a few MHz/mA. All the RoF TXs utilized, as well as the MZM, were operating in C band ($\lambda = 1550\,\mathrm{nm}$). The purpose of utilizing these three different ways to generate the RoF signal was to confirm the influence of the adiabatic chirp factor K_f on $\Delta I_{\mathrm{RFout}}(t)$. The input RF power was $C_{\mathrm{RF}IN} = 0\,\mathrm{dBm}$ ($I_{\mathrm{RF}} = 6.32\,\mathrm{mA}$ since the input port of the laser transmitter was matched on 50 Ω) in all the cases considered. This value of I_{RF} determined three different values of the OMI in the three configurations just described, given, respectively, by $m_I = m_{I1} = 0.085$, $m_I = m_{I2} = 0.085$, and $m_I = m_{I,MZM} = 0.11$. As mentioned in Section 2, in order to put into evidence the influence of the adiabatic chirp factor K_f, a normalization on the value of m_I has been performed for the quantity $\Delta I_{\mathrm{RFout}}(t)$, like what we have done for Fig. 1.

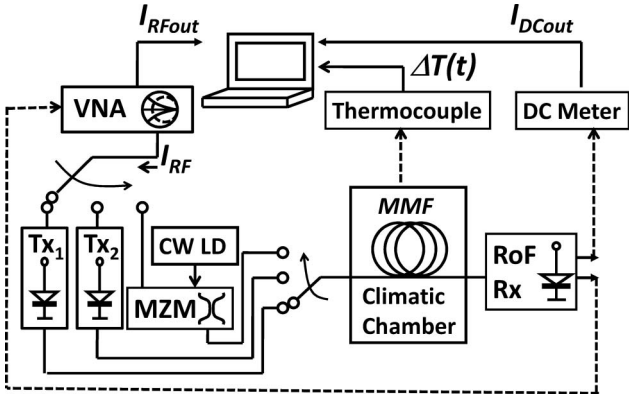

Fig. 2. Experimental setup. See text for details.

We performed our measurements utilizing different values for the frequency of the RF modulating signal. In fact, f_c varied from $f_{c,\min} = 700\,\mathrm{MHz}$ to $f_{c,\max} = 2100\,\mathrm{MHz}$ with steps of $\Delta f_c = 100\,\mathrm{MHz}$. All these values of f_c fell inside the 3 dB bandwidth of the MMF channel and exhibited the same phenomena that we are describing in this work. The reported results refer to $f_c = 1000\,\mathrm{MHz}$.

To put ourselves in a repeatable situation, we decided to induce variation on $\varphi_m(t, L)$, described in Section 2, by forcing a temperature change in the environment of the MMF. The MMF was thus inserted in a climatic chamber and underwent a controlled variation of temperature, whose values were measured by a thermocouple (see Fig. 2).

Figure 3 shows the time behavior of the amplitude of the received RF current compared with the DC for a RoF TX exhibiting $K_f = K_{f1} = 220\,\mathrm{MHz/mA}$. The behavior of the environmental temperature variation ΔT in the same time span is reported in order to put into evidence its correlation with the fluctuations of RF and DC currents. The same behavior that was illustrated with reference to the simulated results in Fig. 1 can now be fully compared to the experimentally achieved results in Fig. 2. Starting again from the instant $t = 0\,\mathrm{s}$ and arriving to $t \approx 400\,\mathrm{s}$, temperature T exhibits an upward sloping behavior, which induces different $\varphi_m(t, L)$ values in the MMF. At this point, the effect of the frequency chirp of the laser source that has been described in Section 2 can be easily observed. In fact, $\Delta I_{\mathrm{RFout}}(t)$ and $\Delta I_{\mathrm{DCout}}(t)$ are not in phase; however, due to the presence of the term proportional to K_f,

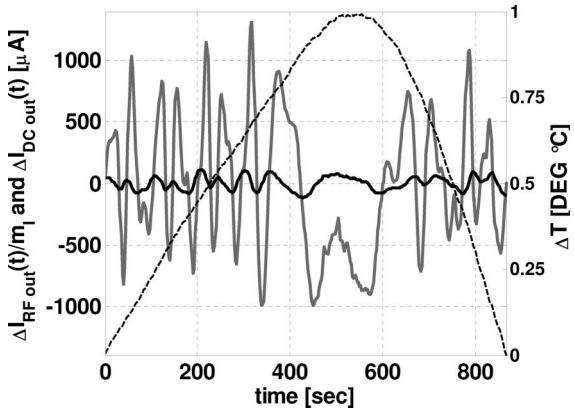

Fig. 3. Behavior of experimentally measured time fluctuations due to modal noise on the amplitudes of the received photocurrent (DC term, black curve; RF term, $f_{RF} = 1\,\mathrm{GHz}$, gray curve) for the RoMMF system considered and of the environmental temperature (dashed curve). The RoF TX used operates in the third optical window and exhibits $K_f = 220\,\mathrm{MHz/mA}$.

$\Delta I_{\mathrm{DCout}}(t)$ exhibits maxima in correspondence to the upward slope of $\Delta I_{\mathrm{RFout}}(t)$. Also in this case, it can be seen that, for $t \approx 400\,\mathrm{s}$, in a span of time of about 200 s, corresponding to a stationary behavior of T (and corresponding to a relatively stationary behavior of the various $\varphi_m(t,L)$), $\Delta I_{\mathrm{RFout}}(t)$ and $\Delta I_{\mathrm{DCout}}(t)$ tend to be relatively stationary. Subsequently, starting from the instant $t \approx 600\,\mathrm{s}$ and arriving to $t \approx 850\,\mathrm{s}$, T exhibits a downward sloping behavior, which induces an opposite time behavior of the various $\varphi_m(t,L)$ in the MMF. As already observed in Section 2, $\Delta I_{\mathrm{RFout}}(t)$ and $\Delta I_{\mathrm{DCout}}(t)$ are also in this case not in phase, and $\Delta I_{\mathrm{DCout}}(t)$ now exhibits maxima in correspondence to the downward slopes of $\Delta I_{\mathrm{RFout}}(t)$.

Note that, to compare measured and modeled values of quantities such as the just described $\Delta I_{\mathrm{RFout}}(t)/m_I$ and $\Delta I_{\mathrm{DCout}}(t)$, or $\Delta I_{\mathrm{RFNORM}}$ and $\Delta I_{\mathrm{DCNORM}}$, which will be introduced below with reference to Figs. 6 and 7, it has been necessary to estimate the values of the surface integrals b_{mn} of Eq. (13). To this purpose, a preliminary work was performed with the aid of our numerical model to determine appropriate values for these unknown parameters. In fact, we did not have detailed data available to model the RoF RX utilized, like the distance L_{PD} between the MMF end section and S_{PD}, the value of S_{PD} and the possible misalignment M_{PD} between the MMF end section and S_{PD}. We only knew that it was a multimode pigtail receiver with no focusing system. We therefore fixed arbitrarily $L_{\mathrm{PD}} = 0\,\mu\mathrm{m}$ and performed a brute force simulation, letting S_{PD} and M_{PD} vary within wide ranges of values in order to find the $(S_{\mathrm{PD}}, M_{\mathrm{PD}})$ pairs that fit all the measured data both for $i_{\mathrm{RFout}}(t)$ and $i_{\mathrm{DCout}}(t)$. The standard deviations of $i_{\mathrm{RFout}}(t)$ and $i_{\mathrm{DCout}}(t)$, normalized to their respective average values, were taken as the quantities to be fitted by our model. More than one $(S_{\mathrm{PD}}, M_{\mathrm{PD}})$ pair was found to satisfy the conditions required. However, the relative differences among them were very small and, consequently, we took for our simulation program the average values among them ($S_{\mathrm{PD}} = 23\,\mu\mathrm{m}$, $M_{\mathrm{PD}} = 1\,\mu\mathrm{m}$), which, in our equivalent RoF RX configuration, appropriately fit all the experimental data.

Figures 4 and 5 show results relevant to cases where the frequency chirp has a lower impact with respect to the case of Fig. 2 ($K_f = K_{f2} = 30\,\mathrm{MHz/mA}$ and $K_f = K_{f,MZM}$, namely, a few MHz/mA, respectively).

In Fig. 4, it can be observed that the "lead–lag" relationship between $\Delta I_{\mathrm{RFout}}(t)/m_I$ and $\Delta I_{\mathrm{DCout}}(t)$ is still present. The term, which in the expression of $\Delta I_{\mathrm{RFout}}(t)/m_I$ is proportional to $\sin(\Delta\varphi_{mn}(t))$, still plays a role, although, it tends to lose relative weight with respect to the term proportional to $\cos(\Delta\varphi_{mn}(t))$.

An important consequence that can, however, be observed is that, with respect to the behaviors seen in Fig. 3, the lower value of K_f gives rise to a more similar range of $\Delta I_{\mathrm{RFout}}(t)/m_I$ variation when compared with $\Delta I_{\mathrm{DCout}}(t)$.

Observing Fig. 5, it can be seen that, due to the very low value of the frequency chirp exhibited by the MZM, the DC and RF fluctuations are in phase since they are both almost proportional to $\cos(\Delta\varphi_{mn}(t))$. Moreover, in this figure, it can be observed that the behavior of $\Delta I_{\mathrm{RFout}}(t)/m_I$ is now practically coincident with $\Delta I_{\mathrm{DCout}}(t)$, as we expect from the theoretical result of Eq. (23).

To represent this important dependence, namely, the fact that the strength of the undesired amplitude variations of $\Delta I_{\mathrm{RFout}}(t)$ grows with K_f, we plotted the values of $\Delta I_{\mathrm{RFout}}(t)/m_I$ versus $\Delta I_{\mathrm{DCout}}(t)$ in the three situations considered (CW RoF TX followed by a MZM, RoF TX with $K_f = 30\,\mathrm{MHz/mA}$, and RoF TX with $K_f = 220\,\mathrm{MHz/mA}$).

To enable the comparison among the three lasers, we have chosen to consider $\Delta I_{\mathrm{RFNORM}} = \Delta I_{\mathrm{RFout}}(t)/|\Delta I_{\mathrm{DCout}}|_{MAX}/m_I$ and $\Delta I_{\mathrm{DCNORM}} = \Delta I_{\mathrm{DCout}}(t)/|\Delta I_{\mathrm{DCout}}|_{MAX}$ instead of $\Delta I_{\mathrm{RFout}}(t)/m_I$ and $\Delta I_{\mathrm{DCout}}(t)$ because, in the three experimental configurations,

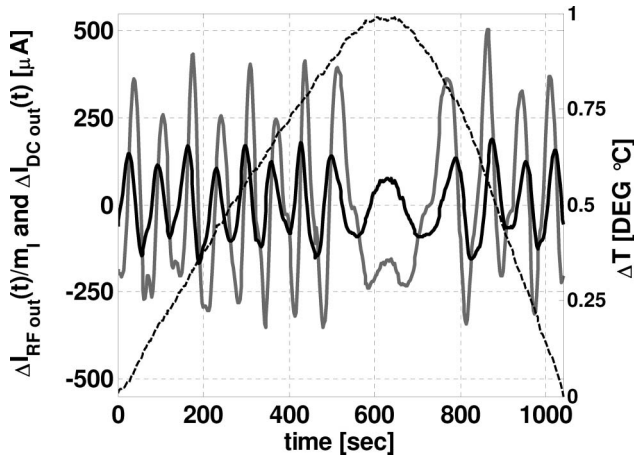

Fig. 4. Behavior of experimentally measured time fluctuations due to modal noise on the amplitudes of the received photocurrent (DC term, black curve; RF term, $f_{RF} = 1\,\mathrm{GHz}$, gray curve) for the RoMMF system considered and of the environmental temperature (dashed curve). The RoF TX used operates in the C band and exhibits $K_f = 30\,\mathrm{MHz/mA}$.

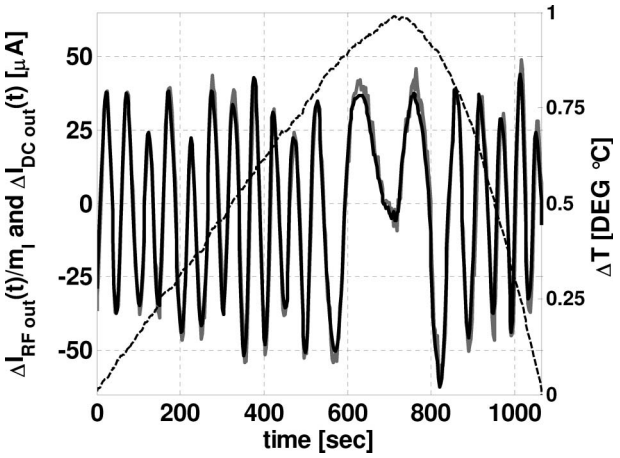

Fig. 5. Behavior of experimentally measured time fluctuations due to modal noise on the amplitudes of the received photocurrent (DC term, black curve; RF term, $f_{RF} = 1\,\mathrm{GHz}$, gray curve) for the RoMMF system considered and of the environmental temperature (dashed curve). The RoF TX used operates in C band and is followed by a MZM, whose frequency chirp can be estimated to correspond to a value K_f lower than a few MHz/mA.

we have different received optical power levels and slightly different temperature changes.

Consequently, Figs. 6 and 7 show, respectively, the measured values and the numerically modeled values of the described quantity $\Delta I_{\mathrm{RFNORM}}$ as a function of $\Delta I_{\mathrm{DCNORM}}$ in the three cases considered.

Starting from Fig. 6, it can be seen that in the case of the MZM-based link, the resulting curve resembles a collection of linear segments, in agreement with what had been observed in Fig. 5, where $\Delta I_{\mathrm{RFout}}(t)/m_I = \Delta I_{\mathrm{DCout}}(t)$.

When the frequency chirp coefficient of the RoF TX increases to $K_f = 30\,\mathrm{MHz/mA}$ and to $K_f = 220\,\mathrm{MHz/mA}$, the corresponding curves turn from a linearlike behavior to elliptical-like behaviors with

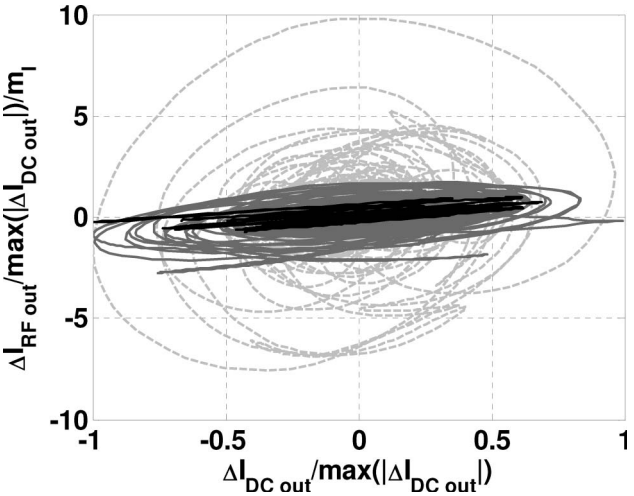

Fig. 6. Behavior of the measured values of $\Delta I_{\mathrm{RFNORM}}$ with respect to $\Delta I_{\mathrm{DCNORM}}$ for the RoMMF system considered. The modulating frequency is $f_{RF} = 1\,\mathrm{GHz}$. Black curve, MZM-based RoF TX; solid gray curve, directly modulated RoF TX with $K_f = 30\,\mathrm{MHz/mA}$; dashed gray curve, directly modulated RoF TX with $K_f = 220\,\mathrm{MHz/mA}$. All RoF TXs operate in C band.

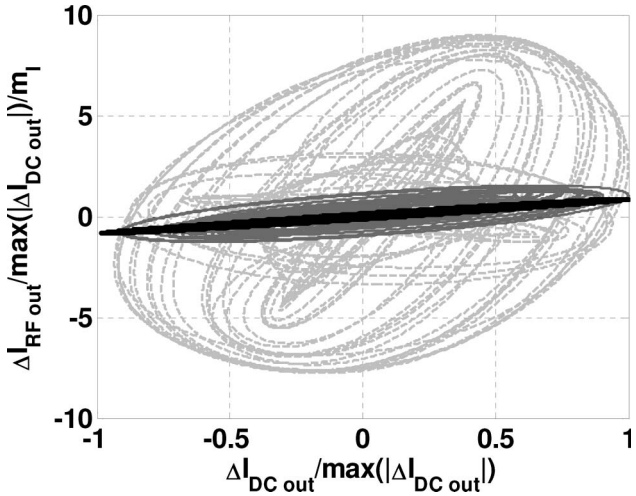

Fig. 7. Same as Fig. 6, but coming from simulated results.

an increasing distance between the maximum and the minimum in the vertical direction. This illustrates the fact that the variation of $\Delta I_{\mathrm{RFNORM}}$ exhibits increasingly higher ranges of variation than the ones corresponding to the MZM-based link.

Utilizing the expression of $\Delta G_{\mathrm{RF}MAX}$ introduced in Eq. (25), it can be noted that these higher ranges of variation of $\Delta I_{\mathrm{RFout}}(t)/m_I$ correspond to a maximum value of the link gain fluctuation, which, in the cases of $K_f = 30\,\mathrm{MHz/mA}$ and $K_f = 220\,\mathrm{MHz/mA}$, is, respectively, about 1 and 4 dB higher than the value corresponding to the case of the MZM-based link. Moreover, from the analysis of Fig. 6 it can be seen that the numerical results are in very good agreement with the experimental measurements.

As a further check between modeled and measured behaviors, we have repeated our simulations considering different $(S_{\mathrm{PD}}, M_{\mathrm{PD}})$ pairs, which had previously all been determined with the brute force simulation described above. A very weak dependence on the chosen $(S_{\mathrm{PD}}, M_{\mathrm{PD}})$ pair has been found, giving reliability to the comparison performed. This can be explained with the fact that, for each $(S_{\mathrm{PD}}, M_{\mathrm{PD}})$ pair, $\Delta I_{\mathrm{DCout}}(t)$ and $\Delta I_{\mathrm{RFout}}(t)$ are both similarly affected by the resulting values of the surface integrals b_{mn} [see Eqs. (6), (12), and (21)], which, in turn, influence in a similar manner both numerator and denominator of $\Delta I_{\mathrm{RFNORM}}$ and $\Delta I_{\mathrm{DCNORM}}$.

Finally, we add that the importance of the phenomena described has been confirmed also with reference to RoMMF links operating in the second optical window. Behaviors similar to those represented in Figs. 3–5 could, in fact, be observed with reference to a 300 m RoMMF link utilizing a DFB laser emitting at $\lambda = 1309\,\mathrm{nm}$ directly and externally modulated, respectively.

4. Conclusion

An accurate analysis has been performed on analog modulated RoMMF links in the particular case of short connections (e.g., a length of a few hundred meters). A model has been developed that allows to put

into evidence the relationship between the varying optical phase differences among the different propagating modes (due to variations of fiber temperature, mechanical stress, etc.) and the time behavior of the undesired amplitude fluctuations of the received photocurrent.

Through an accurate comparison of experimental and modeled results, the numerical model has been successfully tested, confirming an interesting relationship between the fluctuations caused by modal noise on the amplitudes of the DC and of the RF components of the received photocurrent.

Finally, it has been shown that the frequency chirp of the RoF transmitter plays an important role in determining the detrimental effects arising from modal noise, this being the case even considering short-range connections, as the adiabatic chirp coefficient K_f directly contributes to the range of variation of the fluctuations of the RF received photocurrent.

Part of this work has been sponsored by the European Community's Seventh Framework Programme (FP7) under project 212 352 ALPHA "Architectures for fLexible Photonic Home and Access networks." A complementary sponsorship by the Italian Ministry of Instruction is gratefully acknowledged, as well.

References

1. C. Carlsson, A. Larsson, and A. Alping, "RF transmission over multimode fibers using VCSELs—Comparing standard and high bandwidth multimode fibers," J. Lightwave Technol. **22**, 1694–1700 (2004).
2. M.-L. Yee, Y.-X. Guo, V. H. Pham, and L. C. Ong, "WiMedia ultra-wide band transmission in radio over fiber using multimode fiber," *The 20th Annual Meeting of the IEEE Lasers and Electro-Optics Society, 2007* (IEEE, 2007), pp. 335–336.
3. Y. Ma, Y. Tang, and W. Shieh, "107 Gbit/s transmission over multimode fibre with coherent optical OFDM using centre launching technique," Electron. Lett. **45**, 848–849 (2009).
4. M. Webster, L. Raddatz, I. H. White, and D. G. Cunningham, "A statistical analysis of conditioned launch for gigabit ethernet links using multimode fiber," J. Lightwave Technol. **17**, 1532–1541 (1999).
5. M. Duser and P. Bayvel, "2.5 Gbit/s transmission over 4.5 km of 62.5 μm multimode fibre using centre launch technique," Electron. Lett. **36**, 57–58 (2000).
6. R. E. Epworth, "Modal noise—causes and cures," Laser Focus **17**, 109–115 (1981).
7. T. Kanada, "Evaluation of modal noise in multimode fiber-optic systems," J. Lightwave Technol. **2**, 11–18 (1984).
8. R. Dandliker, A. Bertholds, and F. Maystre, "How modal noise in multimode fibers depends on source spectrum and fiber dispersion," J. Lightwave Technol. **3**, 7–12 (1985).
9. E. G. Rawson, J. W. Godman, and R. E. Norton, "Frequency dependence of modal noise in multimode optical fibers," J. Opt. Soc. Am. **70**, 968–976 (1980).
10. A. M. J. Koonen, "Bit-error-rate degradation in a multimode fiber optic transmission link due to modal noise," IEEE J. Sel. Areas Commun. **4**, 1515–1522 (1986).
11. G. C. Papen and G. M. Murphy, "Modal noise in multimode fibers under restricted launch conditions," J. Lightwave Technol. **17**, 817–822 (1999).
12. G. Tartarini and P. Faccin, "Efficient characterization of harmonic and intermodulation distortion effects in dispersive radio over fiber systems with direct laser modulation," Microw. Opt. Technol. Lett. **46**, 114–117 (2005).
13. I. Gasulla and J. Capmany, "Modal noise impact in radio over fiber multimode fiber links," Opt. Express **16**, 121–126 (2008).
14. I. P. Kaminow, T. Li, and A. E. Willner, *Optical Fiber Telecommunications V A: Components and Subsystems* (Academic, 2002).